Making a multi-material leading edge for natural-laminar flow

Erik Kappel[a,*], Olaf Steffen[a], Manuel Buggisch[a]

[a] *DLR, Institute of Lightweight Systems (SY), Lilienthalplatz 7, 38108 Braunschweig, Germany*

DOI: https://doi.org/10.57965/59jw-9388

Abstract

Natural laminar flow (NLF) on the wings' upper surfaces and leading edges is considered one of the most effective approaches to reduce fuel-consumption for next-generation aircraft. The aerodynamic drag can be substantially reduced when NLF is realized. However, even for environmentally friendly, next-generation aircraft, part manufacturing, assembly and maintenance must be affordable. Thus, achieving NLF-ready composite part quality is only one side of the coin. Having design concepts, which assure affordability and maintenance-readiness, is the other side. This whitepaper reports on activities in context of making NLF-ready composite wing structures of the German Aerospace Center's Institute of Lightweight Systems, which were executed within the NACOR project (Clean Sky 2). The article focuses on the making of a full-scale multi-material composite leading edge component.

Keywords: Composite leading edge, Natural laminar flow, Process-induced distortions, Tool compensation

1. Introduction

Composite structures are state of the art for primary structures of modern aircraft as an Airbus A350. Increasing aircraft efficiency by reducing fuel-consumption is an omnipresent ambition nowadays. Reducing drag by realizing natural laminar flow (NLF) on the wings upper surface and the leading edge is considered one of the most effective approaches.

However, the NLF surface requirements are almost impossible to meet with today's structural designs for leading edges (LE) and today's assembly concepts which feature rivet-based wing-cover attachments. Positive and negative steps, small gaps at the leading-edge-to-wing-cover interface and also fastener head marks on the upper-wing-cover's surface scotch natural laminar flow. A discontinuity of a few tenth of a millimeter is already a show stopper for NLF. Therefore, new part designs with accompanying assembly concepts are mandatory to achieve robust NLF for aircraft generations to come.

Integral structural concepts have been proposed by SAAB in the past, which combine the wings' upper wing cover with the leading edge [1], omitting the critical interface area. However, when bird-strike incidents or the typical LE-erosion is considered, fully-integral designs, made from monolithic composite materials, are rather critical from a maintenance perspective, as easy interchangeability is not given and repair is most-often a costly alternative.

DLR's institute for composite structures and adaptive systems is working on the topic of carbon-fiber-epoxy-composite wing components for NLF for almost a decade. The pursued concept features an interchangeable LE, which provides NLF conditions on the surface, on the upper wing cover and - likely most important - across the NLF-critical interface area between both components. The concept addresses today's requirements of interchangeability [6]. After creating an integrally-made bi-directional- stiffened wing-cover in LaWiPro project (see Figure 1a) [10, 11, 12] the studies' focus was turned towards leading edge design and in particular on joining concepts which fulfill NLF requirements and allow for interchangeability at the same time (see Figure 1b).

(a) Upper wing cover (b) Leading edge studies

Figure 1: Results from DLR studies

* Tel.:+49 531 295 2398; fax. +49 531 295 2232
Email address: erik.kappel@dlr.de (Erik Kappel)

The present whitepaper reports on recent DLR's studies in the European project NACOR (see Acknowledgements section) which aim to realize an interchangeable multi-material leading edge, which provides NLF conditions. The particular focus of this document is on the fabrication of the LE, related analyses of process-induced distortions of the multi-material design, the mandatory tool-compensation measures and the final validation by means of experiments and full-scale assembly studies.

2. Ambition and leading edge facts

The outer surfaces of the wing-cover and the corresponding leading edge are deduced from a research wing-configuration, which has been provided by Airbus within the LaWiPro research project [10, 11, 12]. The examined structure represents an outboard wing section with 2.3 m length and a chord length of about 1.8 m, as shown in Figure 2. The wing cover (see Figure 1a) is an integrally stiffened (bi-directional) monolithic carbon-fiber-reinforced-plastic (CFRP) structure, which is made in a one-shot process. The structure combines the outer wing skin with stringers and ribs.

The corresponding LE design pursues a multi-material philosophy, as can be seen in Figure 1b, as a consequence of erosion-protection requirements for the outer surface. Nevertheless the LE component is made in a one-shot autoclave curing process, avoiding secondary bonding or co-bonding processed for cost reasons. The outer LE surface is made from a 0.12 mm thick stainless steel layer which provides appropriate erosion resistance, which typically cannot be achieved with monolithic CFRP laminates, due to their brittle epoxy resin surfaces. Six plies of glass-fiber-fabric and a single layer CFRP fabric prepreg in-between are located underneath the steel layer. This sub laminate mimics a structurally integrated wing-ice-protection-system (WIPS), which is a core part of the pursued LE concept. Detailed investigations on this WIPS system can be found in [4]. Project boundaries and cost reasons led to the decision to implement a WIPS-dummy laminate for the full-scale LE studies presented here, as the primary focus within NACOR is on the validation of interchangeability while fulfilling NLF requirements.

The base laminate of the LE is a monolithic CFRP laminate. It is composed of sixteen plies of a unidirectionally stiffened carbon-fiber-epoxy prepreg (HexPly M21/T800 [13]). The laminate stacking is symmetric with nominal laminate thickness of 4.2 mm.

Figure 3 shows a sketch of the LE's cross section and its attachment to the wing-cover. As a consequence of the challenging NLF tolerances (see Figure 4), fastener marks needed to be eliminated from the upper wing-cover surface, which led to the particular mounting concept, in which the LE attachment is located at the stiffeners of the wing cover. To assure a smooth path of the CFRP base laminate around the critical interface area, a glass-fiber wedge has been introduced. It fills the clearance between

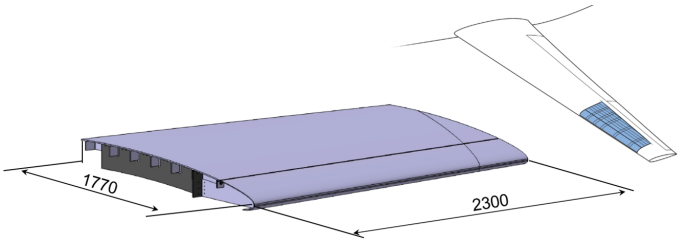

Figure 2: Examined outboard wing section, containing upper wing cover (see Figure 1a), composite ribs and the full-scale LE

the steel layer and the base structure. A sharp bend of the CFRP base laminate had to be avoided in order to prevent resin-rich areas and non-optimal kinks of the fiber paths.

The wedge-area design was examined in a dedicated study within NACOR, focussing on through-thickness strains due to chemical shrinkage of the curing resin. As the wedge height after curing directly affects the particularly important step height at the interface, it represents a key-area for the NLF requirement (see Section 4).

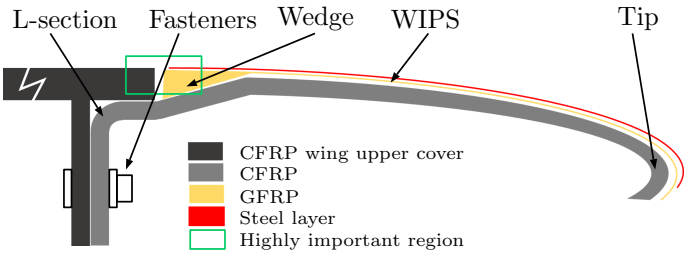

Figure 3: LE cross section with zones and laminate areas

The step height from the LE outer surface to the wing cover's outer surface is utilized for formulating the NLF tolerance corridor, as shown in Figure 4. In earlier projects a step tolerance of $^{+0.5}_{-0.1}$ mm was pursued. However, the recent activities aim for achieving an even reduced corridor of $^{+0.3}_{-0.1}$ mm, as indicated in Figure 4.

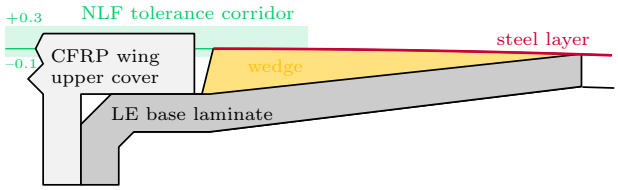

Figure 4: NLF tolerance corridor basis on the step definition. Note that the clearance between the LE and the wing-cover will be filled with appropriate filler material.

2.1. Multi-material approach

As shown in Figure 3, the LE has three different areas from a material perspective, which are described in Table 1. These three sections are composed of the four materials given in Table 2.

Table 1: Material sections within the structure

Section	Specification
CFRP	Monolithic section $[45, -45, 90, (-45, 45)_2, 0]_s$ layup
WIPS	six glass-fabric layers with a single carbon-fabric layer in between
Steel	Single outer steel layer

Table 2: Raw materials used for the LE

Material	Layer thickness
Stainless steel sheet 1.4310	0.120 mm
M21/T800s UD prepreg	0.262 mm
M21 46280 fabric prepreg	0.310 mm
M21/56%/1080 glass-fiber-fabric prepreg	0.066 mm

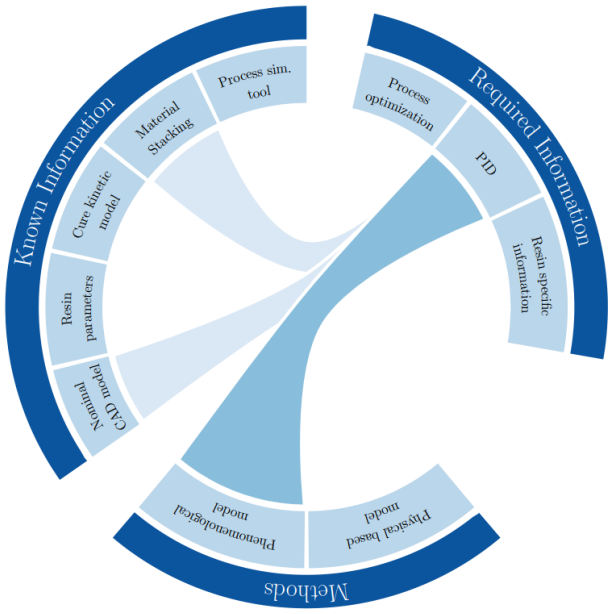

Figure 5: Supplier scenario faced by project engineers

The LE is manufactured in a one-shot autoclave curing process using a female Invar tool (Ni36 alloy), whose design and characteristics are presented in Section 7.

3. FE analyses & parameter deduction

The engineers working in the project were facing the typical supplier scenario (see [14] for details), which is illustrated in Figure 5. The project focus was on making a full-scale leading edge, with excellent dimensional fidelity, in order to serve for the targeted assembly tests (see Section 8) of the NACOR project. Prepreg and other materials were available for manufacturing trials, but detailed material characterizations, to use multi-scale multi-physics approaches were neither available nor considered in the project schedule and budget plans. Thus, a phenomenological-numerical approach, which focusses on predicting part distortions, was pursued (similar as shown in [14]). The pursued strategy and its final application is outlined hereafter in detail.

3.1. Challenge multi-material design

Making non-flat CFRP structures in tight dimensional tolerances is challenging as structures inevitably show process-induced distortions (PID). Adequate tool compensation is mandatory to compensate for material related distortion phenomena. This is also true for the multi-material leading edge examined here. In the present case, however, the situation is even more challenging as most areas of the leading edge show asymmetric laminate stackings. Those are often avoided in composite design due to their challenging accompanying effects in terms of coupling between extension and curvature.

Tool compensation measures need to account for spring-in distortions [5], due the orthotropic nature of the composite material and asymmetry-induced deformations. Irreversible contributions due to the resin's curing-related chemical shrinkage need to be considered. Reversible distortions, due to the orthotropic thermal expansion, with its strong dominance of strains in the laminates' resin-dominated through-thickness direction, need also be anticipated. These contributions are superposed by distortions coming from the asymmetric stacking sequence.

The cross-section distortions of a cylindrically curved monolithic CFRP structure can be described with the well-known model proposed by Radford [15], which describes the angle change $\Delta\varphi$ of a curved section with an initial enclosed angle $\tilde{\varphi}$ based on the strains acting in tangential ε_T and through-thickness direction ε_R[1] of the laminate.

$$\Delta\varphi = \frac{\varepsilon_T - \varepsilon_R}{1 + \varepsilon_R} \cdot \tilde{\varphi} \tag{1}$$

This relation allows for considering contributions due to thermal expansion as well as chemical shrinkage. Typically a superposition is assumed, as shown hereafter.

$$\begin{aligned} \frac{\Delta\varphi}{\tilde{\varphi}} &= \frac{(\alpha_T - \alpha_R)\,\Delta T}{1 + \alpha_R \Delta T} + \frac{\varepsilon_T^{ch} - \varepsilon_R^{ch}}{1 + \varepsilon_R^{ch}} \\ &= reversible + irreversible \end{aligned} \tag{2}$$

In fact, thermal contribution to the overall part distortions act in a reversible manner. Magnitudes change with

[1] Denoted as radial direction in Radford model, which is in fact usually equal to the laminate's through-thickness direction

temperature. In contrast, fractions induced by the curing process of the epoxy resin are irreversible. They do not change with temperature. Radford's analytical model allows for determining spring-in values for a 2D circularly curved section. But in order to apply it to full 3D structures, FE modeling is mandatory as the LE structure is neither circularly curved nor a profile with constant cross-section.

In order to model both contributions in an FE simulation simultaneously it is convenient to combine both effects by using effective CTE parameters. This, allows the user to use available material descriptions with the commercial FE tools. Thus, using $\alpha_R^{effective}$ allows for modeling both contributions.

$$\frac{\Delta\varphi}{\tilde{\varphi}} = \frac{\left(\alpha_T - \alpha_R^{effective}\right)\Delta T}{1 + \alpha_R^{effective}\Delta T} \quad , \tag{3}$$

while ΔT refers to the temperature step from curing to room temperature (-155 °C here). Classical laminate-theory is capable to capture the effect of asymmetric stacking on part shape.

$$\begin{bmatrix} \varepsilon_x \\ \varepsilon_x \\ \gamma_{xy} \\ \varkappa_x \\ \varkappa_y \\ \varkappa_{xy} \end{bmatrix} = \begin{bmatrix} [A] & [B] \\ [B] & [D] \end{bmatrix}^{-1} \cdot \begin{bmatrix} \vec{N}_T \\ \vec{M}_T \end{bmatrix} \tag{4}$$

$$= \begin{bmatrix} \vdots & \vdots & \vdots & \vdots & \vdots & \vdots \\ \vdots & \vdots & \vdots & \vdots & \vdots & \vdots \\ \vdots & \vdots & \vdots & \vdots & \vdots & \vdots \\ \vdots & \vdots & \vdots & \vdots & \vdots & \vdots \\ \vdots & \vdots & \vdots & \vdots & \vdots & \vdots \\ \vdots & \vdots & \vdots & \vdots & \vdots & \vdots \end{bmatrix} \cdot \begin{bmatrix} \vec{N}_T \\ \vec{M}_T \end{bmatrix} \tag{5}$$

However, CLT is related to shell-element-based modeling in FE models, which typically cannot capture 3D distortion effects such as spring-in, which is driven by through-thickness strains. Therefore, solid-element modeling becomes mandatory, to address both, spring-in distortions as well as effects due to asymmetric laminate stacking (see Section 6.1 for details).

3.2. Simulation-parameter calibration challenge

TMA tests have been performed to characterize the different prepreg materials. These tests provide insight in the thermal-expansion characteristic. However, comprehensive mechanical characterization of the individual prepregs were out of the project scope for cost and time reasons. In addition, standard procedures to quantify chemical-shrinkage-induced distortions are not available.

Therefore, a two-path strategy has been created to determine the required simulation parameters. As describe in the following section the pursued concept is based on distortion comparison between multiple simple-shaped samples and corresponding numerical models. The FE models utilized data-sheet information for Engineering constants while the through-thickness effective CTE was subject of calibration until a satisfactory match between experimentally measured distortions and corresponding numerical predictions is achieve. In this process, it is particularly important that the determined parameter set provides satisfying prediction accuracy for all different sample configurations.

3.3. Simulation-parameter calibration based on optimization

The stress-free temperature T_{sf} during the process is a key information when it comes to tool compensation. T_{sf} describes the moment during the curing process when the resin starts to transfer relevant loads.

As the LE has symmetric monolithic sections as well as hybrid areas with asymmetric stacking the parameter determination process is more challenging as multiple distortion phenomena interact.

The pursued concept features three steps. First, TMA tests were performed for determining the 3D CTE values for the materials used in the LE structure. In the second step, a finite-element analysis is coupled with an optimization algorithm. The FE model features four different circularly-curved samples (see Figure 6), with deviating stackings. Circular geometry was used, as is allows for the easy quantification of radius changes (3-node-evaluation). In the third step, the analyzed configurations were created in an autoclave process, while effective distortions were evaluated based on optical scans of the fabricated structures.

The optimization approach, was to minimize the average deviations over all four samples, while the parameter $\alpha_R^{effective}$ was to be optimized.

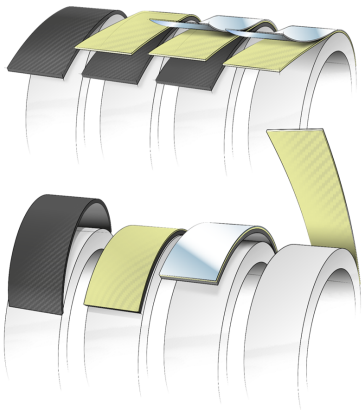

Figure 6: Material combinations in the different LE zones and corresponding zone-specific distortion modes. Black, yellow and silver indicate CFRP, WIPS and the steel layer, respectively. The bottom picture shows the expected principle distortions after the curing process.

Samples of the specific Prepregs were fabricated and TMA tests were performed to determine 3D laminate and ply CTEs for the planned simulations Figure 7 gives insight in the TMA-sample-creation process.

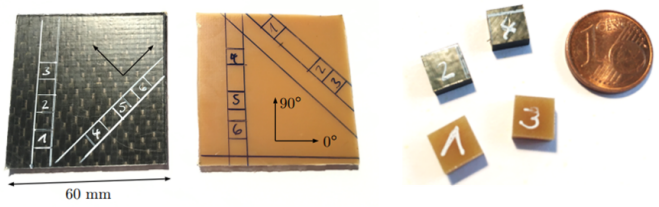

Figure 7: TMA sample creation for specific materials. Global laminate CTEs α_x, α_y and 45° rotated laminate CTEs are measured.

CTEs testing was executed in accordance with the proposed CTE-determination procedure described in [16], which aims to improve comparability between individual testing campaigns. The determined results are shown in Figure 8,

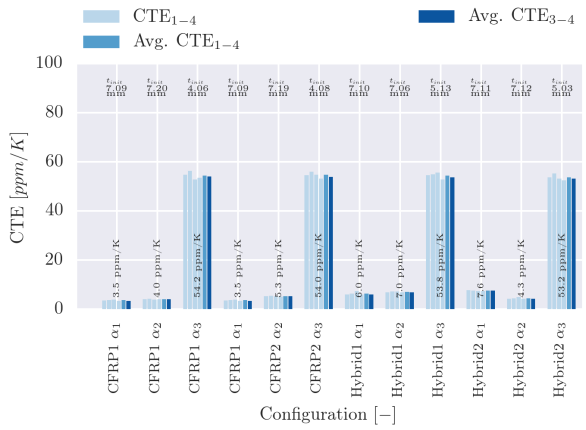

(a) CTEs of the base laminate (CFRP) and the Hybrid section

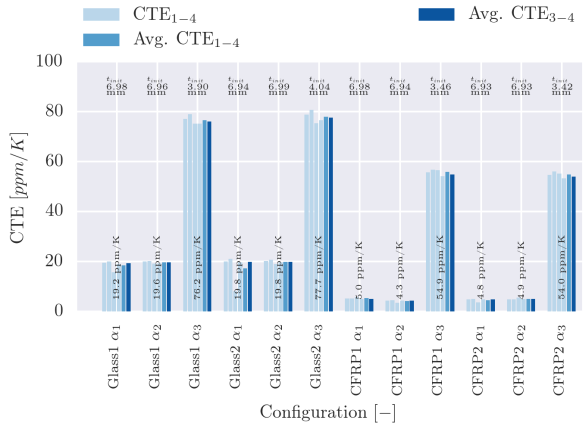

(b) CTEs of the WIPS related raw materials

Figure 8: Determined laminate CTEs for the specific materials

while Table 3 shows the determined laminate CTEs.

Table 3: CTE results for the LE materials

Prepreg	Layup	α_x	α_y	α_z
M21/T800s #1	cross ply	4.8	4.9	54.0
M21/T800s#2	cross ply	5.0	4.3	54.9
M21 46280 #1	cross ply	3.5	4.0	54.2
M21 46280 #2	cross ply	3.5	5.3	54.0
M21/56%/1080 #1	cross ply	19.2	19.6	76.2
M21/56%/1080 #2	cross ply	19.8	19.8	77.7

The quasi-isotropic nature of the laminates leads to $\alpha_x \approx \alpha_y$. The high thermal expansion along the resin-dominate through thickness direction $\alpha_z \gg (\alpha_x, \alpha_y)$ is a clear outcome of the test. In addition, the tests clearly show the even higher CTE values of the GFRP laminate, which is a consequence of the higher glass-fiber CTEs.

The shape of the curved sample (from Figure 6) after manufacturing can be seen in Figure 9. Note, that flat samples (F1, F2) were also manufactured. Those were made to uncouple spring-in distortion from asymmetry effects. They are also shown in Figure 9 but not further discussed here.

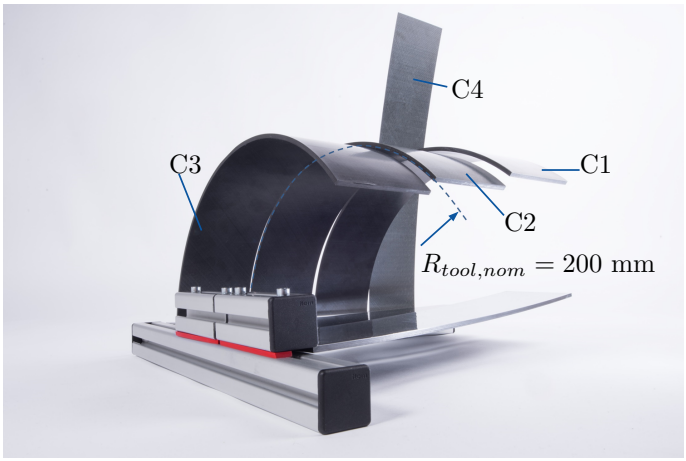

Figure 9: Distortions of manufactured samples. Note that all parts were made on the same circular aluminium pipe with a nominal 200 mm radius.

Table 4 provides information on the stackings of the created samples. Figure 10 shows de FE model and a deformation plot. The FE model combines all four curved samples in a single assembly, as this eases the Python-script-based deformation evaluations.

Table 4: Manufactured specimens. Note, that the WIPS section is composed of a $[G_3, C, G_3]$ laminate, while G and C denote glass-fabric and CFRP-fabric prepreg layers, respectively.

Specimen	Steel 0.120 mm	WIPS 0.706 mm	CFRP 4.192 mm
C1	x	x	x
C2		x	x
C3			x
C4	x	x	
F1	x	x	x
F2			x

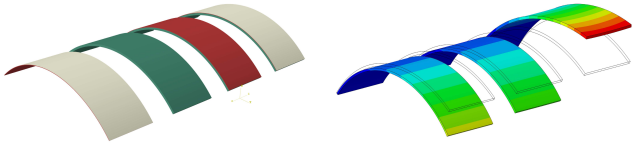

(a) FE models (b) Deformation

Figure 10: Modeling curved samples. Note that the C4 sample was not used for the fitting as the configuration is not representable for the LE configurations

The deformation shown in Figure 9 allowed for preliminary assessments. Configuration C3 represents a monolithic symmetric laminate. A radius reduction is found as a consequence of spring-in distortions. Configuration C2 combines C3 with the WIPS area. The laminate is asymmetric. As the WIPS CTE in hoop direction, increases the CFRP CTE, the cool down leads to a radius increase. For C2 it was found that spring-in distortion and the asymmetry-induced effect compensate each other almost completely, leading to part shape close to the tool shape. C1 represent the full laminate, which basically adds a steel layer to C2. Due to the comparably high steel CTE, the outward bending increases, leading to an over-compensation of spring-in distortion, thus, producing a part with a global radius larger than the tool radius.

The C4 configuration combines the steel layer with the WIPS section. As can be seen in Figure 9, the C4 configuration produced almost flat part indicating the strong asymmetry-induced effect.

The described scenario has been executed in multiple loops, while Table 5 contains the developed data set, which has been used for the further activities in context with the full-scale LE.

Table 5: Updated parameter set for application to full leading edge

Property	CFRP	WIPS	Steel
E_{11} [GPa]	43.5	41.6	195.0
E_{22} [GPa]	43.5	41.6	195.0
E_{33} [GPa]	10.3	10.0*	195.0
G_{12} [GPa]	34.0	16.4	75.6
$G_{13} = G_{23}$ [GPa]	54.4	30.0*	75.6
ν_{12} [-]	0.54	0.265	0.29
ν_{13}, ν_{23} [-]	0.21	0.30*	0.29
α_{11} [ppm/K]	4.1	8.7	15.0
α_{22} [ppm/K]	4.1	8.7	15.0
α_{33}^{**} [ppm/K]	116.848	116.848	15.0

4. Wedge effect analysis

The step height at the wedge area is the key parameter for NLF, as it determines whether a smooth transition between the LE and the wing cover shall be realized. A dedicated study has been executed to experimentally derive the adequate tool dimension for the step, in order to meet the exact laminate thickness of the wing cover laminate after curing.

Figure 11 shows an excerpt of this study. Flat samples were created which mimic the step at the wedge area. These samples feature the final layup architecture of the LE. The created specimens were examined based on optical measurements (GOM Atos system). In addition a comprehensive micro-section analysis was executed to quantify the realized step height at the wedge area. The global shape analysis shows a consistent effect, which induces a slight upwards bending of the samples. This finding was important. It strongly affects the LE shape, as a tipping movement is induced. This leads to the fact, that the wedge-are needed to be incorporated for the FE analyses for the full-scale LE.

5. Tool compensation

Whenever non-flat composite structures shall be made in tight dimensional tolerances, the nominal tool shape needs to adapted to compensate for the inevitably occurring shape changes of the composite structure, which are a consequence of the material's orthotropic character. The compensation procedure is not a linear problem [7]. However, often adequate parts can be obtained when precalculated distortions are used for the adaptation of the nominal tool shape, as it has been experimentally verified for a CFRP box structure in [7].

Manufacturers have the following options for determining their compensation measures.

- Experience-based compensation

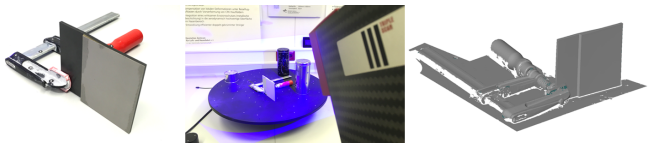

(a) Wedge specimen optical inspection using [17]

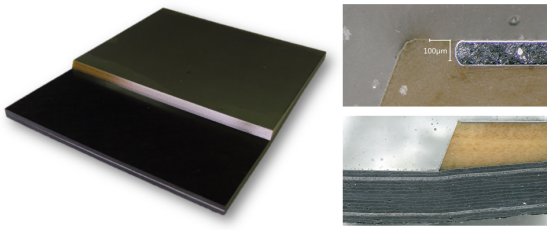

(b) Micro section analysis of wedge area

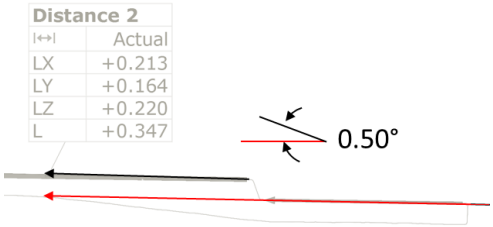

(c) Wedge-related distortion

Figure 11: Wedge area analyses excerpt

- Full 3D compensation based multi-scale, multi physics models
- Full 3D compensation based phenomenological-numerical models
- Pragmatic compensation, which focusses on compensating the most-relevant distortions with simple compensation measures

Which approach is best depends on the problem at hand, available resources and available expertise. The LE at hand is considered challenging, as the typical composite-specific distortions are superposed by effects related to the asymmetric stacking sequence and the multi-material design. Therefore, experience-based compensation approaches were hardly applicable for the LE component.

A direct tool-shape compensation, based on the 3D simulation results presented above, was considered critical, as the double-curvature of the outer surface would have been modified locally, leading to the potential issue that the initially flat steel layer cannot follow the contour of the compensated tooling, leading to gaps. The necessity of plastic pre-stretching of the 0.12 mm steel layer could have been a conceivable consequence, which was not tested before. This steel-layer pretreatment is considered detrimental to the whole LE concept due to the related costs, transport and storage issues of the this pre stretched steel foils, which cannot be rolled to a coil after pre-stretching. To assure the validity of the NACOR manufacturing concept, which has been experimentally verified (see Figure 13), a pragmatic compensation strategy was pursued for the LE at hand. The compensation measures are derived from full 3D data sets which are determined with the P-approach concept presented in [8].

5.1. Small scale LE demonstrator

In line with the aerospace building-block approach, numerical models as well as specimens and structures of different scales and complexity were examined on the path towards the full-scale LE component. The parameter determination procedure and the application of the P-approach are described in detail in Section 3. To verify the determined effective parameters a small-scale LE demonstrator configuration has been developed from the final LE shape. The demonstrator structure is 400 mm long. It shows all features of the full-scale LE in terms of laminate stacking and the multi-material architecture. Figure 12 shows its location in relation to the full-scale LE.

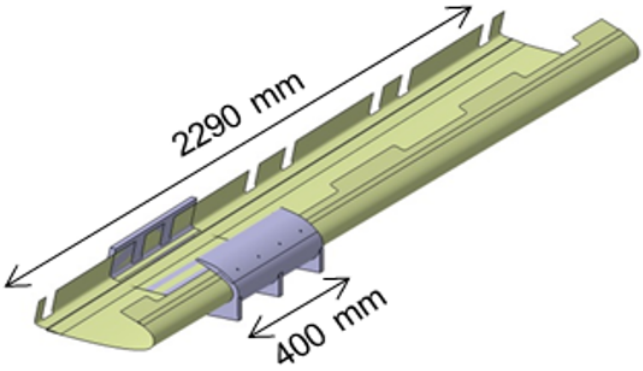

Figure 12: Small-scale leading edge demonstrator source

The demonstrator has been used to verify the developed manufacturing process and the tool design (see Section 7) on the one hand, as shown in Figure 13.

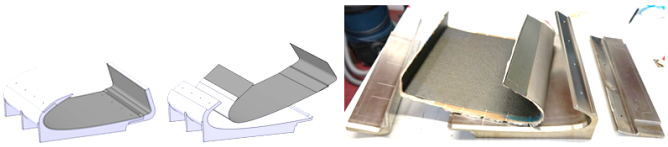

Figure 13: Small-scale 400 mm leading edge manufacturing

On the other hand, it was used to verify the PID predictions, prior the simulation concept is applied to the full-scale LE. The validation concept pursued the idea to compare the shape of a demonstrator, which is manufactured in a nominal-shape tool, with a corresponding numerical prediction that utilizes the determined parameters.

Multiple demonstrator structures were created. Optical measurements with a GOM Atos [17] system were

performed to examine the structures' shape after manufacturing. Figure 14 shows the measurement procedure using a rotating table and the determined digital representation.

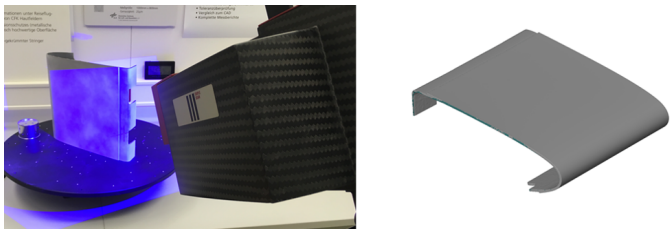

Figure 14: Full-field scans were taken from the small-scale LE using a GOM ATOS system [17]

The LE's outer surface is examined to assess prediction accuracy. The FE model is described in Section 3. It is the same for the small-scale demonstrator and the full-scale LE. The node coordinates of the outer surface of the numerical model were extracted from the result file. This data set is used within the GOM Inspect software to execute the comparison. The nodes are used for a mesh creation, which is utilized to perform a surface comparison between the nominal part shape and the present shape.

Figure 15 shows the determined results, while the same legend boundaries are shown. The qualitative shape is predicted excellently, while a slight under prediction is observed in the areas dominated by asymmetry effects.

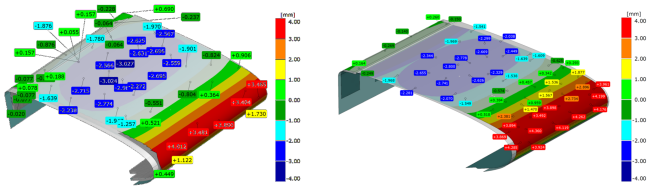

(a) Optical measurement (b) FE simulation result

Figure 15: Measurement and Simulation result for the small-scale LE

These results were used to update the initial simulation parameter set until satisfying prediction accuracy was achieved. These parameters were later used to calculation PID of the full-scale LE. The result of the small-scale Demonstrator already allows for identifying the most relevant distortion modes, which will also affect the full-scale LE. Figure 16 summarizes the most relevant modes based on a representative cross section.

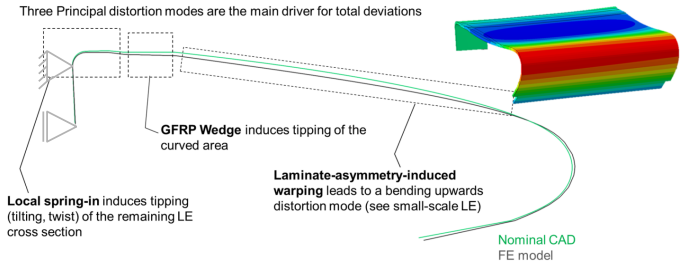

Figure 16: Distortion modes of the small-scale LE

The analysis revealed the following relevant compensation measures.

- Spring-in compensation of monolithic CFRP L-section
- Compensation of upwards tilting, induced by the GFRP wedge (see Section 4)
- Curvature increase along the hybrid section to compensate for the upwards bending mode due to layup asymmetry and multi-material design

6. Full-scale leading edge

Performing PID analyses for full-scale CFRP structures requires solid-element-based FE simulation models, in order to capture all relevant distortion-inducing phenomena. Therefore, an FE model has been created for the full-scale leading edge based on the nominal geometry of the part, coming from a surface model in CATIA CAD tool.

6.1. FE model specs

The FE model has been set up in ABAQUS CAE. It is shown in Figure 17. The full-scale model features 50462 20-node brick elements (C3D20), wherein the different material sections are considered as homogenized. The utilized material properties are summarized in Table 5.

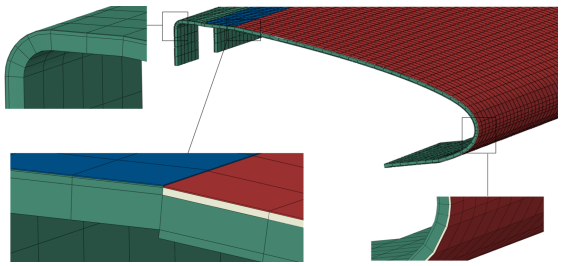

Figure 17: FE model for full-scale LE. Red, beige, green and blue indicate the steel layer, the WIPS section, the CFRP section and the CFRP-wedge area, respectively

The effective CTE $\alpha_R^{effective} = \alpha_3 = \alpha_z$ has been utilized in order to capture thermal and chemical contributions to the overall distortion. The simulation was set up with a single static simulation step, in line with

the phenomenological-numerical simulation approach. For sake of tool compensation, all nodes being part of the aerodynamic surface and its extension to the L-bend area were considered. Figure 18 shows the determined deformations magnitudes.

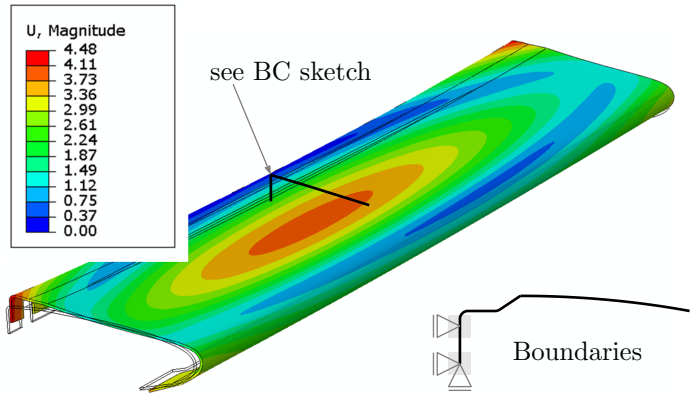

Figure 18: Distortions magnitudes of the full-scale LE. Distortion given in mm (displayed 20x magnified). No gravity considered in model.

Appropriate boundary conditions were assigned to the L-bend area of the center-cross-section to prevent free-body movements (see Figure 18). Gravity effects were not captured in the initial simulation step, which was focussed on quantifying the PID characteristic as a consequence of the curved shape and the asymmetric multi-material layup.

6.2. Assembly-force estimation

The wing-cover/leading edge interface can be described by a straight line. The asymmetric multi-material stacking leads to a bending mode of the LE structure, as shown in Figure 18, which is not compensated due to the steel-layer limitations discussed above. Whether this effect is critical for the whole assembly, needs to be assessed. A dedicated FE model has been created which builds up on the PID model. The new model constraints the global bending mode of the LE by boundary conditions, assigned at the interface area. In fact, vertical displacements are constrained. An analysis of the reaction forces allows for estimating assembly forces, which will be necessary to compensate the global bending when the LE is joined with the upper wing cover. Figure 19 shows the simulation results, where the reaction forces in vertical direction are given in Newton.

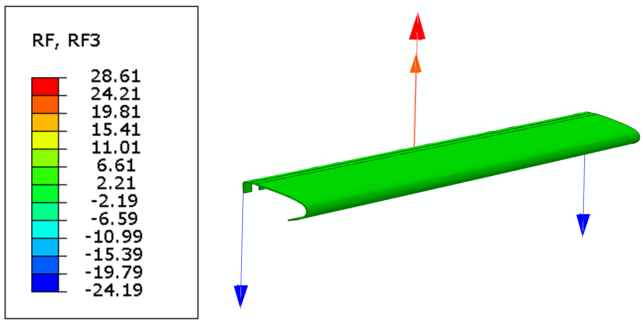

Figure 19: Assembly-force estimations with RF3 values given in N.

Only, three nodes were used in order to determine maximum point loads. The shape of leading edge, being an open profile from a mechanical perspective, results in relatively low resistance against bending and twist. Thus, the determined reaction forces are rather low, as expected. With respect of the final project aim, which is to perform repeated assembly tests, while the NLF criteria are assessed at the LE-to-Wing Cover interface, it was concluded that the determined forces are acceptable.

As discussed indicated above, a holistic three-dimensional compensation of the nominal shape of the whole LE was not pursued within the NACOR project, due to differently weighing of the project outcomes. The main project aim was to create full-scale LE samples, which should be used in assembly demonstrations (see Section 8). Full-three-dimensional shape compensation of the nominal LE shape would lead to a complex shaped, doubly curved tool shape. This creates the potential risk, that the thin sheet-metal layer cannot be formed to the tool surface, due to its high stiffness. Neat resin flow between the steel layer and the tool-surface was feared, which would led to unacceptable parts. Due to project schedule and budget limitations, there was no capacities to experimentally examine the particular scenario of a doubly-curved tool surface. Therefore, a non-conventional compensation concept was pursued, which should improve the dimensional fidelity of the LE sample, but does not necessitate comprehensive changes of the experimentally verified manufacturing process.

Nonetheless, the verification of the applied phenomenological -numerical PID prediction process was an important topic in the project to assess whether successful compensation can be expected for cases when full 3D compensation is executed. This effort is mandatory as part-distortion compensation by tool shape modification is a non-linear phenomenon per definition, as it is outlined in [7]. A multi-step approach has been executed for verification. It combines two different numerical predictions with the nominal surface, pursuing the aim to validate the compensation idea. Figure 20 summarizes the executed process. The study features two different model states. The first state represents the PID prediction, known from

Figure 18. A surface comparison between the simulation results (only nodes on the aerodynamic surface) and the nominal part surface are executed within the GOM inspect software, where distances between the nominal and the deformed surface are quantified. Figure 22a shows the determined result. Note that in Figure 22a distances are illustrated. Those refer to the normal direction of the measured surface, which is a remarkable difference to Figure 18 which displays node translation magnitudes[2].

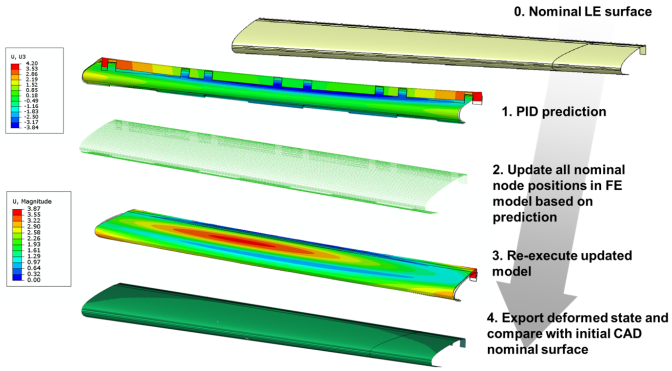

Figure 20: Two-step numerical validation of the derived compensation measures

Therefore, Figure 22a gives an impression of part-shape deviation magnitudes which need to be expected, when no tool-shape compensation is executed. To examine the effect of a full 3D tool compensation, the simulation results of the first-state model are utilized. As common in a basic tool-compensation process, the determined deformations are 'subtracted' from the nominal shape. In practice, this requires the export of node-specific translation vectors from the first-state model. These vectors were first oriented in the opposite direction and then added to the nominal node coordinates of the state-one model. This minimizes model setup effort, as the step back to the CAD system and a CAD & FE model re-creation could be avoided. The created state-2 model has been executed and the deformed shape of the aerodynamic surface, with the attached L-bend, has been exported for assessing the quality of the compensation against the nominal part.

Figure 21 shows the result of this comparison.

[2]Important comment: Displacement in FE models always refer to a global simulation coordinate system. The displacements does not refer to distance measured with respect to the nominal part surface.

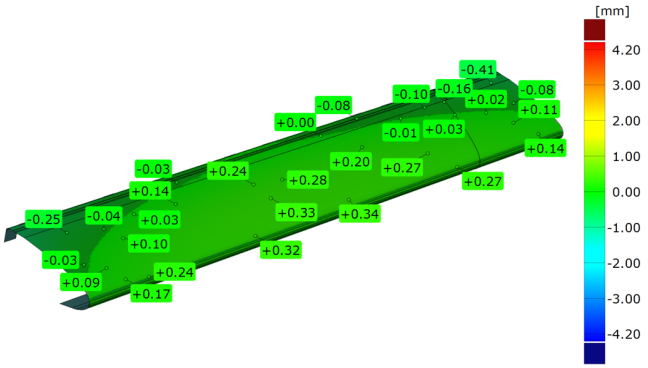

Figure 21: Assessing the effect of tool compensation of final deviations to nominal shape

The deviation flags quantify the distances of the deformed mesh, referring to the normal direction of the tesselated mesh created from the surface nodes. For sake of comparison the legend has been kept unchanged compared to the state-1 result. It can be seen that excellent compensation results are obtained, all well within a ±0.5 mm corridor. Figure 22 shows the direct comparison of the two model states.

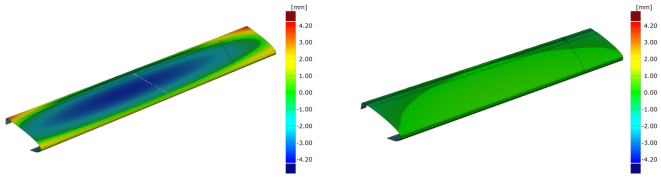

(a) without compensation (b) with compensation

Figure 22: FE result for full-scale LE, verifying the compensation measures numerically

Even though deviation magnitudes of less than ±0.5 mm are acceptable for most structural components, the compensation results can be improved by executing an additional simulation loop, using the deviation of the state-2 model to update the already modified tool surface again. Due this repeated application, which actually can be automated, the final part shape is expected to approach the nominal part shape.

6.3. Applied pragmatic part compensation

Simulation models of the full-scale LE were used to deduced three main compensation features, which have been quantified also based on the accompanying verification studies with the small-scale LE and the wedge-area analysis. The compensation measures refer to the following cognitions:

- The monolithic CFRP L-bend at the attachment are will show classical spring-in distortions, which affect the global position of the whole LE.

- The wedge-area was found to initiate a slight upward tilting due to local laminate asymmetry, induced by the higher GFRP CTE..
- The asymmetric multi-material layup at the curved section leads to an upward bending mode in direction of flight. In the LE's length direction a global curvature is observed whose compensation can be achieved due to assembly forces.

Instead of re-transferring FE results back to the nominal CAD model, the deduced measures were implemented manually in the CAD model. Figure 23 shows the realized compensation measures, where the red surface represents the compensated tool shape.

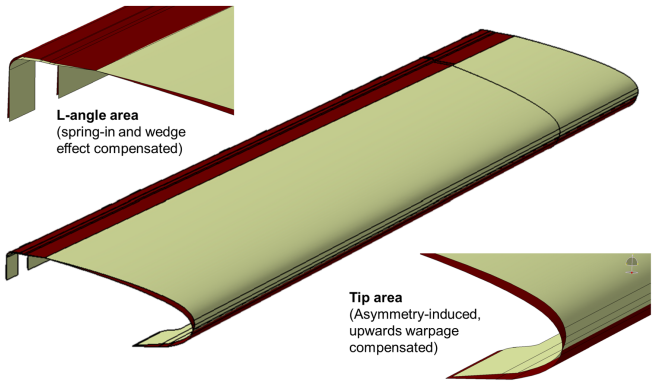

Figure 23: Tool compensation measures, update of nominal CAD design prior tool manufacturing

After an update of the nominal CAD model of the full-scale LE the tool was manufactured. The tool concept and the final tool are shown in Figure 28. The manufacturing strategy, which has been validated for the small leading edge (see Figure 13) has been transferred to larger scale.

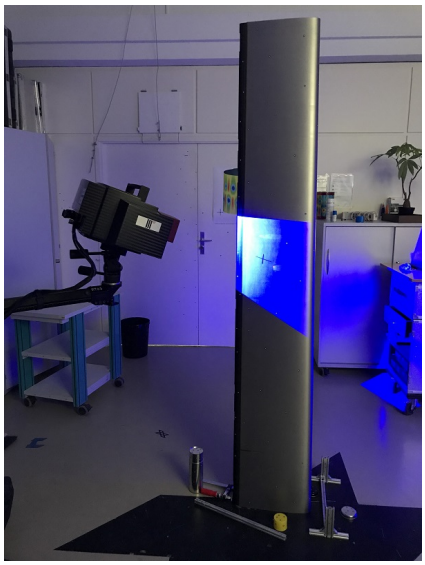

Figure 24: ATOS [17] scan of a single full-scale LE

In total three full-scale LEs were manufactured. Figure 24 shows an excerpt of the quality control process. Surface scans were preformed to assess the dimensional fidelity of the fabricated structures.

Figure 25 shows the comparison between the simulation result and the identified shape of the manufactured full-scale LE #3. The principle distortion mode is well predicted by the numerical model. As compensating the global curvature was not addressed by the defined compensation measures, due to the steel-layer uncertainty, an elimination of global bending was not expected. The measurements shows that the maximum deflections are even slightly underestimated by the simulation.

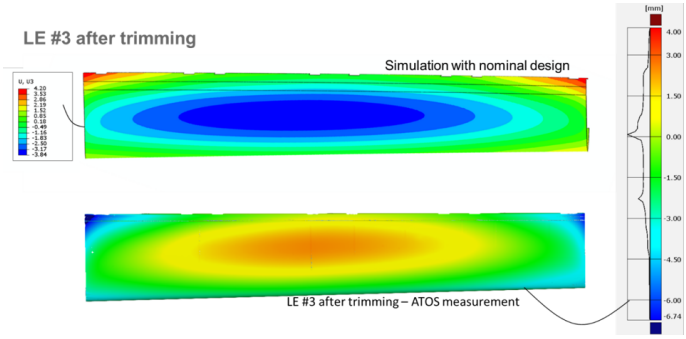

Figure 25: Global shape comparison between simulation and manufactured full-scale LE. Note that global curvature was not compensated intentionally due to project boundaries

To avoid false interpretation due to the superposed global bending of the LE, the center-cross section is evaluated hereafter. Figure 25 shows a qualitative assessment of the center-cross section with respect to the major project aim of a smooth transition at the wing-cover-to-LE interface.

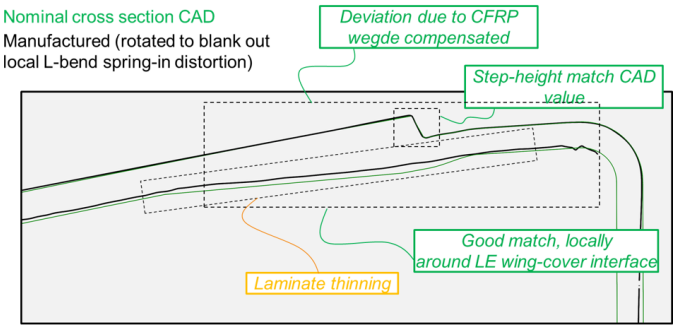

Figure 26: Center cross-section effect assessment. Black cross section refers to the manufactured part. Nominal cross section is shown in green

The comparison shows a satisfying match around the interface area, which indicates a good basis for successful assembly tests. The comparison shows some laminate thinning underneath the wedge area. Further examina-

tion is necessary, utilizing the manufactured small-scale LE samples and the other full-scale LEs. Figure 26 shows the quantitative assessment of the center cross section. Compared with the simulation result, shown in Figure 18 it is concluded that upward warpage has been reduced by the part-shape compensation, but it has not been fully compensated.

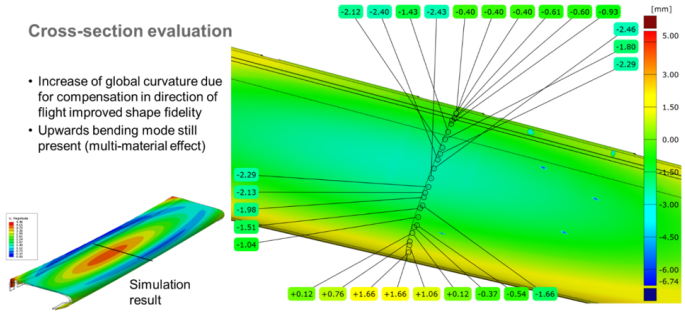

Figure 27: Center cross-section deviations. The small-illustrated simulation result refers to Figure 18

6.3.1. Lessons learned

CFRP-specific effects, as Spring-in affect the LE design but play a minor role for the whole part. Distortions are dominated by laminate-asymmetry effects. The applied pragmatic compensation approach improved the overall shape conformity. With focus on the planned assembly study in NACOR, which focus on verifying NLF ready conditions at the wing-cover-to-LE interface, before and after exchanging an LE device the following key points were identified. Geometry evaluations show:

- Step height of the wedge area is met, leading to the aspired smooth transition to wing cover expected for assembly tests.
- Satisfying match between CAD shape and manufactured part shape at the interface area is observed.
- Global bowl shape in direction of flight is reduced by compensation, but not fully eliminated.
- Effect of the CFRP wedge (local upward rotation in direction of flight) cannot be identified in the evaluated cross sections anymore.
- Global part bending in span wise direction is still present, as it was intentionally not addressed in compensation. However, due to the open-profile character of the LE, forces to compensate for global bending are small, creating no issues for planned assembly tests.
- Full-3D compensation conceivable based on the simulation results. However, additional studies to answer the uncertainty regarding the steel layer and its application in combination with more complex curved tool surfaces

7. Manufacturing tool design

The LE is manufactured in a single-sided tool concept, using a female tool on the outer surface. The tool design focusses on an efficient process sequence, combining a male preforming tool, and a sectioned female tool made from Ni36 steel (Invar). The tool assures adequate and precise handling, which is necessary to assure excellent laminate quality. In particular the joining of the full prepreg stack with the steel-layer, which is aligned in the female tool beforehand demands for precise operation, which could be achieved with linear guides. Figure 28 shows the developed tool concept and its final realization.

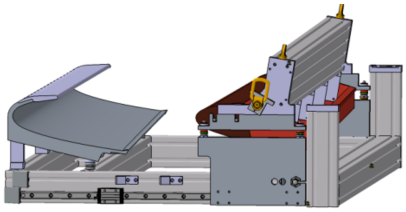

(a) Tool design

(b) Realized tool

Figure 28: Tool design for full-scale LE manufacturing

The female tool is sectioned at the L-angle area, in order to ease the insertion of the preform tool and to allow for simple demolding. After the L-angle section is attached to the main tool, the preform tool is removed, leading to a single-sided manufacturing setup in the end. Bagging is applied directly on the Invar female tooling. The curing process is executed in an 180 °C autoclave process according to the MRCC of Hexcel for the utilized prepregs.

8. Outlook

Validating an NLF-ready interchangeable leading edge concept is a considerable challenge, as this article shows.

However, interchangeability and NLF has additional facettes, which demand for further investigation. As a consequence of the different aircraft states, as for example in cruise condition or on ground tanked, wing bending differs drastically. In order to examine and finally underline the concepts maturity, DLR pursued the idea of an assembly demonstrator. The CAD model and the final demonstrator are shown in Figure 29.

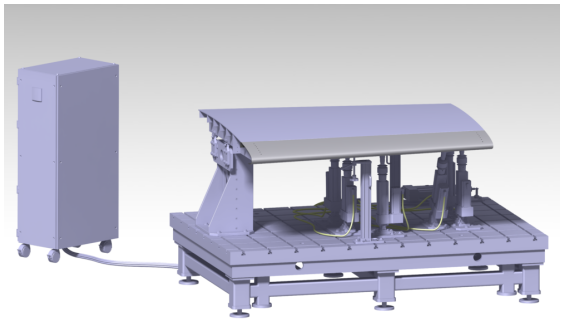

(a) CAD Model of test stand

(b) Final test stand with wind cover section and the mounted leading-edge sample

Figure 29: Assembly demonstrator for verifying interchangeability under NLF requirements.

The demonstrator allows for applying realistic wing-bending modes to the structural assembly, consisting of the wing-cover shown in Figure 1a, the attached full-scale LE and additional interconnecting elements (ribs, LE supports). The demonstrator pursues the following aims

- Assessing the NLF-ready transition area between LE and wing cover for in-flight wing shape
- Demonstrating and validating the developed interchangeability concept
- Examining the interchangeability for on-ground conditions under maximum wing-bending

9. Conclusion

The present article sheds lights on the challenge of making a composite leading edge component, which provides an NLF-ready transition to a wing-upper cover. Erosion protection requirements and the need for an anti-icing system led to a multi-material design approach for the leading edge component, which features a CFRP base laminate, an integrated electric anti-icing system and a stainless steel outer surface layer. One-shot manufacturing is considered the most cost-efficient approach. However, the multi-material concept, complicates the tool-design and manufacturing drastically, as spring-in and laminate-asymmetry-induced part deformations need to be considered in detail, in order manufacture a part which meets the specified nominal shape. The present whitepaper reports on preliminary studies, the compensation challenge and the finally applied pragmatic compensation approach, which was executed for the full-scale NACOR leading-edge component.

It shall be highlighted that similar in-depth reports, for accompanying topics, were also created in NACOR (see. [20, 21, 22]). A final scientific article summarizes the wide topic range of the project, has been published recently [19] in 2024.

Acknowledgements

The NACOR project has received funding from the Clean Sky 2 Joint Undertaking under the European Union's Horizon 2020 research and innovation programme under grant agreement No CS2-AIR-GAM-2014-2015-01. The work builds on previous nationally funded (LuFo, BMWI) research projects LaWiPro (FKZ: 20W0910A), MOVE_ON (FKZ: 20A1101B), LDAinOp (FKZ: 20A1302B), Impuls-Effekt (FKZ: 20W1526E)

References

[1] Nyman T, Hörberg E. Shape Distortion Analysis of a Complex Shaped Wing Skin Section, DOI: 10.13140/RG.2.1.2784.7847, 2015

[2] Giddings PF, Bowen CR, Salo AIT, Kim HA, Ive A. Bistable composite laminates: Effects of laminate composition on cured shape and response to thermal load. Composite Structures 92;2220-2222, 2010

[3] Lamineries MATTHEY SA. Steel 1.4310 Data sheet. Issue 3.01 - 2006/08

[4] Pototzky A. GraphenunterstÃ¼tzte Konstruktionsmethode zur Funktionsintegration in Leichtbaustrukturen. PhD thesis (Publication in progress). Technical University of Braunschweig, 2020

[5] Kappel E. A study on composite frame distortions due to processing, thermal loads and trimming operations and an assessment from an assembly perspective. Composite Structures 220;338-346, 2019

[6] Steffen O, Ückert C, Kappel E, Bach T, Hühne C. A Multi-material, Multi-functional Leading Edge for the Laminar Flow Wing. 27th SICOMP Conference, Linköping, May 30.-31. 2016

[7] Kappel E. Compensating process-induced distortions of composite structures: A short Communication. Composite Structures 192; 67-71, 2018

[8] Kappel E, Stefaniak D, Fernlund G. Predicting process-induced distortions in composite manufacturing: A pheno-numerical simulation strategy. Composite Structures, Vol. 120, pp. 98-106, 2015

[9] Kappel E. Process Distortions in Composite Manufacturing. PhD Thesis, Otto-von-Guericke University Magdeburg, Germany, 2013
[10] Apmann H et al. LaWiPro - Laminar CFRP-Wing shell production : Abschlussbericht https://doi.org/10.2314/GBV:783152590, 2013
[11] Hansen H et al. LaWiPro - Laminarflügel in CFK-Bauweise: Auslegung, Design und Validierung. Airbus Operations, https://doi.org/10.2314/GBV:790809982 , 2013
[12] Hühne C et al. Abschlussbericht LaWiPro (Laminar Wing Production). https://doi.org/10.2314/GBV:78372439X , 2013
[13] Hexcel. HexPly M21E /34% /UD134 /IMA-12K. Product Data Sheet, Hexcel Corporation, 06/2015
[14] Kappel E. A zone-based approach to predict process-induced distortions of composite structures based on a 'spring-in reference curve'. Composite Structures 209:143-149, 2019
[15] Radford DW. Shape Stability in Composites. PhD Thesis. Rensselaer Polytechnic Institute, 1987
[16] Kappel E. On thermal-expansion properties of more-orthotropic prepreg laminates with and without interleaf layers. Composites Part C: Open Access 3, 100059, 2020
[17] GOM ATOS system. Gesellschaft für Optische Messtechnik (GOM). ATOS manual. https://www.gom.com/de-de/produkte
[18] Steffen O, Meyer P, Hühne C. Natural laminar flow leading edge: Requirements, design, and experimental validation under operational loads. Aerospace Science and Technology 146, 108913, 2024
[19] Buggisch M. Entwicklung eines Fertigungsprozesses für eine Laminare Flügelvorderkante. Deutscher Luft- und Raumfahrtkongress, Bremen, Germany, 2021
[20] Steffen O, Buggisch M, Kosmann J, Kappel E, Köke H, Hühne C. On-ground testing of a laminar flow wing leading edge, https://doi.org/10.25967/550045, 2021
[21] Dähne S, Steffen O, Kosmann J, Hühne C. An automated assessement tool of NLF criteria for airframe joints. https://doi.org/10.25967/570041, 2022.
[22] Heinrich L and Kruse M. Laminar composite wing surface waviness - two counteracting effects and a combined assessment by two methods. https://www.dglr.de/publikationen/2016/420148, 2016.